Applied Catalysis B: Environmental 241 (2019) 270–283

Contents lists available at ScienceDirect

Applied Catalysis B: Environmental

journal homepage: www.elsevier.com/locate/apcatb

Selective hydrodeoxygenation of biomass derived 5-hydroxymethylfurfural over silica supported iridium catalysts

R.J. Chimentão[a,1], H. Oliva[a,1], J. Belmar[b], K. Morales[a], P. Mäki-Arvela[c], J. Wärnå[c], D.Yu. Murzin[c], J.L.G. Fierro[d], J. Llorca[e], D. Ruiz[a,*]

[a] Physical Chemistry Department, Faculty of Chemical Science, University of Concepcion, Casilla 160-C, Concepción, Chile
[b] Organic Chemistry Department, Faculty of Chemical Science, University of Concepcion, Casilla 160-C, Concepción, Chile
[c] Laboratory of Industrial Chemistry and Reaction Engineering, Åbo Akademi University, FI-20500, Turku, Finland
[d] Institute of Catalysis and Petrochemistry (CSIC), Cantoblanco, 28049, Madrid, Spain
[e] Institute of Energy Technologies, Department of Chemical Engineering and Barcelona Research Center in Multiscale Science and Engineering, Universitat Politècnica de Catalunya, EEBE, 08019, Barcelona, Spain

ARTICLE INFO

Keywords:
Iridium
5-Hydroxymethylfurfural (HMF)
Hydrogenation
Hydrodeoxygenation

ABSTRACT

Catalytic performance of iridium supported on SiO_2 was investigated for 5-hydroxymethylfurfural (HMF) transformation. Ir/SiO_2 catalysts exhibiting different metal loading (1, 3, and 5 wt.%) were tested in the preliminary experiments in the hydrogenation of two probe molecules, *e.g.* ethyl pyruvate (EP) and ketopantolactone (KP) to evaluate the Ir dispersion on the catalyst activity in C=O hydrogenation. In the transformation of HMF the influence of metal dispersion, iridium precursor and addition of H_2SO_4 were studied revealing that 2,5-*bis*-(hydroxymethyl)furan (BHMF) was the main product with 83% selectivity at 70% conversion of HMF over chlorine free Ir/SiO_2 together with H_2SO_4 at 333 K in THF under 10 bar H_2 pressure. On the other hand, one-pot synthesis of HMF to 2,5-dimethylfuran (DMF) was promoted in the presence of chlorine containing 1%Ir/SiO_2(Cl) and H_2SO_4. Both of these products are considered high value-added chemicals from biomass-derived 5-hydroxymethylfurfural. The exposed iridium atoms together with the total acid sites are an important catalytic descriptor for hydrogenation of HMF to BHMF.

1. Introduction

Biomass is a sustainable source of renewable chemicals to meet the growing demand for energy [1]. A sustainable production of biobased chemicals in the future depends on the development of new technologies with the desired functional specificity in the transformation of available bioresources [2]. Expected shortages of crude oil will inevitably lead to an increased reliance on coal, natural gas, or renewable sources as feedstocks for the chemical industry. In addition to the shift in the feedstock base, newly developed technologies will have to address other sustainability concerns including environmental impact and energy efficiency [3]. Carbohydrates derived from biomass (primarily cellulosic components of biomass) such as glucose and fructose are economically suitable to be employed as feedstock for the production of useful chemicals (Scheme 1) [4,5].

5-Hydroxymethylfurfural possesses a high industrial potential for production of value-added chemicals (Scheme 1). The most convenient method for the synthesis of HMF is the acid-catalyzed dehydration of fructose [6]. In the recent years, several extensive reviews have showed that chemistry of HMF formation is based on acid-catalyzed dehydration of hexoses. HMF is considered to be the most promising important intermediate for the synthesis of a wide variety of chemicals [7,8].

HMF can be used as a starting point to produce a variety of potential furan derivatives and chemical intermediates. HMF contains three functional groups, namely C=O, O−H and C=C in the furan ring (Scheme 1). In particular a variety of chemicals such as 2,5-dimethylfuran (DMF); 2,5-(dimethyl)tetrahydrofuran (DMTHF), 2,5-*bis*-(hydroxymethyl)furan (BHMF) and 2-hydroxymethyl-5-methylfuran (MFA) (Scheme 2) can be produced via catalytic hydrogenation of HMF. These compounds can be used as six-carbon monomers that could replace petrochemical-based monomers [4]. DMTHF is an ether with several features making it attractive as a fuel component. It has a boiling point of 92 °C and limited solubility in water. Its energy density of 35.5 MJ/kg is higher than that of ethanol (25 MJ/kg) and

* Corresponding author.
E-mail address: doruiz@udec.cl (D. Ruiz).
[1] These authors contributed equally.

https://doi.org/10.1016/j.apcatb.2018.09.026
Received 6 June 2018; Received in revised form 4 September 2018; Accepted 8 September 2018
Available online 11 September 2018
0926-3373/ © 2018 Published by Elsevier B.V.

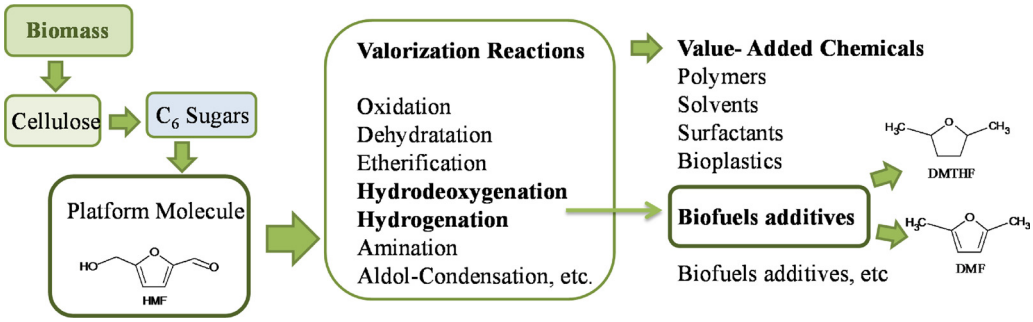

Scheme 1. Biomass transformation to HMF and the reaction network of HMF conversion to chemicals.

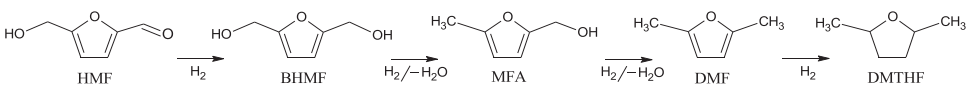

Scheme 2. Overall reaction pathways for conversion of HMF to DMF and DMTHF.

comparable to butanol (36 MJ/kg). Synthesis of DMTHF from biomass by Grochowski et al. [9] raised interest in this compound as a fuel additive. DMF is also an important compound because it has a potential use in gasoline blends and can be converted to *p*-xylene through a Diels-Alder reaction with ethylene [10,11]. DMF has several advantages over ethanol as a gasoline-alternative biofuel. The energy density of DMF (30 kJ cm^{-3}) is higher than ethanol and much closer to that of gasoline which improves mileage for the same size of a fuel tank. Another promising property of DMF is its use as a fuel additive to boost octane number (RON) [12]. It must be added that DMF is completely uncompetitive with the food chain [13].

In the first step in HMF hydrogenation C═O group is hydrogenated to give BHMF. Further hydrogenolysis of this intermediate (BHMF) leads to formation of DMF. The intermediate BHMF has two different types of oxygen atoms; ring oxygen and hydroxyl oxygen and only hydrogenolysis of the latter one yields DMF [14]. Previous work also reported that formation of DMF from BHMF hydrogenolysis occurs via MFA as an intermediate [15]. The first step in HMF hydrogenation is a typical hydrogenation of α,β-unsaturated aldehydes, such as crotonaldehyde and cinnamaldehyde [16]. The previous work in ref [16]. revealed that catalysts for hydrogenation of crotonaldehyde and cinnamaldehyde display selectivity to the unsaturated alcohols in the following order: Os > Ir > Pt > Ru > Rh > Pd. Iridium also exhibited efficient catalytic performance for hydrogenation of HMF carbonyl group [16]. The factors governing intrinsic selectivity of metals have been highlighted by the theoretical calculations of Delbecq and Sautet [17] showing that selectivity over metals can be rationalized in terms of different radial expansions of their *d* bands. The larger is the *d* band, the stronger are the four electron repulsive interactions with the C═C bond and then the lower is adsorption probability. The *d*-band width increases in the series Pd < Pt < Ir. This hypothesis is in line with experimental data for hydrogenation of HMF to BHMF.

Numerous efforts have been devoted to development of hydrogenation catalysts for the production of these furans [18]. One approach is to use formic acid as a chemical hydrogen (H_2) carrier to transform HMF to DMF in addition to presence of H_2SO_4 acting as an acid catalyst [19], although formic acid can also act as a deoxygenation agent of furanylmethanols. Ruthenium and iridium catalysts have been used with formic acid in HMF hydrogenation to DMF [20]. The hydrogenation of HMF with molecular hydrogen is usually performed in an aqueous medium in the presence of supported Ni, Pt, Au, Mo, Sn, Co, Cr, Ru and Ir catalysts under conditions close to 150 °C and H_2 pressure of 5–60 bar. High temperature and pressure can lead to over-hydrogenation of the furan ring or promote undesired side reactions [16,21–23]. Typically, DMF formation was promoted by high reaction temperatures, for example when HMF transformation was performed in THF at 220 °C under 15 bar H_2, HMF hydrogenation gave 78% yield of DMF with complete conversion [24]. In addition, Ru/Co_3O_4 gave 94.1% yield of DMF in HMF transformation at 130 °C under 7 bar H_2 in 24 h in THF as a solvent at more than 99% conversion level [23]. Pt and Pd supported catalysts have been the most commonly used heterogeneous catalysts in the conversion of HMF exhibiting high affinity to C═C transformation. Pd based catalysts possess high activity for hydrogenation of the furan ring. Selective hydrogenation of HMF to BHMF has been demonstrated especially over several Ru, Pt and Cu supported catalysts [25].

In this work Ir/SiO_2 was selected as a catalyst due to its high potential to be as a selective catalyst for transformation of HMF to BHMFs [26,27]. Thananatthanchon et al. [28] found that Ir-based catalysts exhibited outstanding activity for the reduction of HMF to BHMF using FA as *in situ* H-donor, however, these catalysts showed poor tolerance to FA and lost half of its initial catalytic activity within few minutes. In addition, $Ir\text{-}ReO_x/SiO_2$ was very selective (> 99%) in HMF hydrogenation to BHMF at more than 99% conversion level under mild conditions, *e.g.* 30 °C under 8 bar H_2 in 6 h in water [27]. Ir/TiO_2 was also very selective towards BHMF in HMF hydrogenation in water giving the yield of 95.4% at 99.5% conversion level in HMF hydrogenation at 50 °C under 60 bar H_2 in 3 h [26]. Some liquid Brönsted acids such as H_2SO_4 and H_3PO_4 were tested in different systems of biomass derived compounds as a potential strategy to enable an efficient one-pot synthesis of DMF from HMF [29]. The efficiency of reactants is increased in one-pot reactions by avoiding steps of intermediates isolation or changing the reaction conditions [30].

The support is not a mere spectator in HMF hydrogenation, instead directly participating in the reaction [31]. The intrinsic properties of the supports and the metal support interactions affect the catalytic performance. Different supports have been reported in the HMF transformation such as Al_2O_3, chromia, zeolites (HY and NaY) and SiO_2. Alumina is an acidic support which can catalyze secondary reactions such as dehydration, polymerization and cracking leading to coke deposition on the catalyst surface and to blockage of the active sites [32]. Toxicity associated with Cr species in the chromium oxide catalysts necessitates development of a new generation of catalysts [33]. Acidity of zeolites, in particular HY zeolite is responsible for more pronounced side reactions such as ring opening through breakage of the furanic C—O bond being typically catalyzed by Brönsted acid sites [34]. SiO_2 is an excellent candidate as a support due to its high specific surface area. In addition, mesostructured silica is thermally stable and exhibits weak acidic strength [35].

Several solvents exhibiting different chemical nature, have been used in HMF hydrogenation, such as aprotic nonpolar (toluene), aprotic polar (tetrahydrofuran (THF), dimethyl sulfoxide (DMSO) and acetonitrile (CH_3CN)) and protic (2-propanol) were used to investigate the effect of solvent on HMF transformations [24]. Solvents containing

nitrogen (CH_3CN) or sulfur (DMSO) are known to deactivate metal based catalysts due to interactions of the lone pair of electrons on nitrogen/sulfur particularly with the empty *d* orbitals of transition metals [36]. These interactions may result in blocking of metal active sites for HMF adsorption promoting deactivation. Concerning toluene it must be added that toluene and HMF compete for the same active sites thus suppressing HMF conversion [24]. Previous work [37] reported that selectivity to DMF from HMF catalytic transformations in aqueous medium did not exceed 1%. Furthermore, DMF is not soluble in water. The highest catalytic performance for HMF transformations was reported for THF as a solvent [24].

Since Ir supported catalysts have been very scarcely used in selective hydrogenation of HMF to BMHF [26,27], Ir supported on silica was selected as a promising catalyst to investigate the effect of iridium dispersion on hydrogenation of HMF to BHMF using THF as solvent. In the preliminary work the selection of an optimum metal loading in Ir/SiO_2 catalyst was done by hydrogenation of two probe molecules, *e.g.* ethyl pyruvate (EP) and ketopantolactone (KP), which have shown to be very sensitive to the method of the catalyst preparation [38]. After selection of the optimum metal loading for Ir/SiO_2 catalyst, this catalyst was used in selective HMF hydrogenation to BMHF. One of the main aims was to reveal the role of the iridium precursor by using chlorine-containing precursors and a chlorine-free route. Hydrogenolysis of HMF to DMF was also evaluated by combination of iridium catalysts with H_2SO_4, despite of the fact that the presence of strong acid sites may cause side reactions during HMF conversion such as ring opening [39]. An appropriate combination of metal and acid sites may result in a suitable hydrogenation and hydrogenolysis of carbonyl and hydroxyl groups respectively for selective hydrogenation of HMF to DMF [14].

The physical-chemical structure of the iridium catalysts was investigated by a range of physical method including using X-ray diffraction (XRD), N_2-physisorption, transmission electron microscopy (TEM), X-ray photoelectron spectroscopy (XPS), temperature-programmed desorption of NH_3 (NH_3-TPD), temperature programmed reduction (TPR), chemisorption of hydrogen, annular dark-field scanning transmission electron microscopy (HAADF-STEM) and scanning electron microscopy with energy dispersive X-ray spectroscopy (SEM-EDS).

2. Experimental

2.1. Chemicals

All solvents were previously purified by traditional distillation methods and the preparation of catalysts was performed in inert media. Precursors and substrates were used as received.

Ethyl pyruvate (≥98%), ketopantolactone (≥97%), 5-hydroxymethylfurfural (≥98%), toluene (≥98%), *bis*(1,5-cyclooctadiene) diiridium(I)dichloride ($[Ir(\mu\text{-}Cl)(\eta^2\text{-}C_8H_{14})]_2$), 97%) and Iridium(III) acetylacetonate ($Ir(C_5H_7O_3)_3$, 97%), abbreviated as IrClCO and Ir $(acac)_3$ precursors respectively, were purchased from Sigma-Aldrich. Tetrahydrofuran (≥99%), n-hexane (≥99%) and sulfuric acid (98%) were supplied by Merck. Nitrogen and hydrogen, both 99.999%, were supplied by Linde/AGA.

2.2. Catalysts preparation

Ir/SiO_2 catalysts were synthesized from IrClCO and $Ir(acac)_3$ precursors and labeled Ir/SiO_2(Cl) and Ir/SiO_2 catalysts respectively. Preparation was carried out in THF using the evaporation-impregnation method and SiO_2 of the size 100–120 μm. The metal loading on SiO_2 was varied from 1 wt.% to 5 wt.%, synthesizing 1%Ir/SiO_2(Cl), 1%Ir/SiO_2, 3%Ir/SiO_2 and 5%Ir/SiO_2 catalysts. Catalysts were dried and activated by reduction under H_2 (30 mL min^{-1}) for 2 h at 723 K.

2.3. Catalyst characterization

Specific surface area, pore diameter and pore volume were determined from nitrogen adsorption measurements carried out at 77 K in a Micromeritics TriStar 3020 equipment. The samples were first out gassed at 423 K overnight. Calculation of the surface area and pore volume was carried out using Brunauer-Emmett-Teller and Barrett, Joyner and Halenda (BJH) methods, respectively.

DRX analysis was performed on a Bruker diffractometer model D4Endeavor equipped with a Nickel filter and a Cu-Kα X-ray source. The analysis conditions were 40 kV and 20 mA. The diffractograms were recorded in a range of Bragg angles (2θ) between 2° and 90° at 0.02 counts per second.

The transmission electron microscopy analysis was used to study the structural properties and to evaluate the metal particle size of silica supported metal catalysts. TEM analysis was performed in a Jeol Model JEM-1200 EXII Equipment analyzing more than 1000 metallic particles in each sample.

The results obtained by TEM allow determination of the metal dispersion (D) and the diameter of nanoparticles. The specific metal surface area is defined as:

$$S_{Metal} = N_S \times \sigma \times 10^{20} \quad (\mathrm{m^2\,g_{Ir}^{-1}}) \tag{1}$$

Where:

$\mathbf{N_s}$: number of surface metal atoms per gram of metal (atom $g_{Ir}{}^{-1}$)

$\boldsymbol{\sigma}$: Metal atom cross section (for Ir = 7.69 Å^2 atom^{-1}).

The apparent average metal crystal size is obtained from:

$$\bar{d} = \frac{5}{S\,x\,\rho} \tag{2}$$

where

$\bar{d}$: Average metal diameter

5: Number of exposed faces, considering that one of six faces of the metal cubic crystal is attached to the support.

S: is the metal surface area obtained by multiplying the maximum specific surface area (at metal dispersion 100%) which the measured dispersion. For Ir it corresponds to 241 (m^2/g metal).

ρ: is the specific density of the metal 22.56 g/m^3 × 10^6 for Ir.

The dispersion is calculated according to D (%) = $\bar{d}/d_{TEM}$ × 100%, where d_{TEM} is the metal diameter obtained from TEM.

The microscope used for high-angle annular dark-field scanning transmission electron microscopy (HAADF-STEM) and for analysis of Energy Dispersive Spectroscopy (EDS) was a FEI Tecnai F20 equipped with a field emission electron gun and operating at 200 kV. The samples were dispersed in an alcohol suspension and a drop of the suspension was placed over a grid with holey-carbon film.

The acid properties of catalysts were measured by temperature programmed desorption of ammonia. Measurements were carried out using a TPR/TPD 2900 Micromeritics apparatus, equipped with a thermal conductivity detector. The acidity of each catalyst was calculated from the amount of NH_3 desorbed from room temperature to 1223 K at 10 K min^{-1}.

TPR analysis was carried out on a TPR/TPD 2900 Micromeritics apparatus provided with thermal conductivity detector. The carrier gas was 5%H_2/Ar in flow of 40 mL min^{-1} and a heating rate of 10 K min^{-1} from room temperature to 873 K.

The XPS analysis was performed on a Fisons Escalab 200R spectrometer, with a hemispheric analyzer of Mg Kα X-rays radiation source ($h\nu$ = 1253.6 eV), operated at 10 mA and 12 kV. All catalysts analyzed by XPS were pretreated *in situ* in a high pressure cell with H_2 flow at room temperature for 30 min. The binding energies of the XPS spectra were referred to the C1s component (BE = 284.8 eV) and internal Si2p reference (BE = 103.4 eV). The chemisorption analysis was performed

in a Micromeritics ASAP 2020 instrument. The iridium sample was heated in He flow at 400 K for 1 h; then the He flow was replaced by H_2 flow and the temperature was increased to the correspondent reduction temperature (623 K). The iridium sample was reduced for 2 h and subsequently out-gassed for 30 min. Finally the iridium sample was cooled to 310 K and evacuated at 310 K for 30 min. The hydrogen adsorption isotherm was recorded at 310 K. After evacuation at 310 K for 30 min, a second H_2 isotherm was obtained. The chemisorbed H_2 uptake was obtained by the double isotherm method. The number of exposed iridium atoms was calculated assuming spherical particles and stoichiometric factor H/Ir = 1 (atomic chemisorbed hydrogen per surface of iridium atom).

2.4. Catalytic activity tests

Reactions were carried out in a semi-batch glass-lined stainless steel reactor with a volume of 250 mL which was equipped with a heating jacket, a gas inlet, a sampling line and a temperature controller.

Hydrogenation of EP and KP as probe molecules was performed using the initial molar ratio of substrate/Ir of 100/1, under constant pressure of H_2 (10 bar) in 80 mL of toluene at 298 K and stirring rate of 800 rpm. In all experiments, prior to the reaction the loaded reactor was flushed with nitrogen and hydrogen and then pressurized to the desired initial pressure.

Valorization reactions of HMF were carried out under constant pressure of H_2 (10 bar) in 80 mL of THF at 333 K, using a molar ratio HMF/Ir of 100/1 and stirring rate of 800 rpm. Some experiments were performed with an addition of small amount of acid to the reaction media in a molar ratio of HMF/H_2SO_4 equal to 10/1.

In this work an appropriate amount of the substrate was selected based on a preliminary investigation of the HMF/iridium ratio to determine the existence of potential diffusional limitations. In particular 4 experiments were done altering HMF/Ir molar ratio between 50 and 200. The best catalytic results were obtained at HMF/Ir of 100, which was further pursued. In the experiments varying HMF concentrations no major differences in selectivity or activity were found. For an eventual industrial implementation it would be beneficial to perform the reaction at high HMF concentration of even without a solvent.

Recycling tests were carried out in hydrogenation reaction of HMF, recovering and using 3 times the same catalyst in each reaction respectively. The recovered catalysts were washed in 20 mL of n-hexane and dried under vacuum prior to a new use.

The samples from the reactor were withdrawn at different time intervals and analyzed with a GC–MS Clarus 680 and SQ8T-headspace Perkin Elmer equipped with a β-dex column (length 30 m, diameter 225 μm, film thickness 0.25 μm). Helium was used as a carrier gas.

For characterization of the products formed during HMF hydrogenation CG/MS analysis was performed comparing the retention times and corresponding patterns with standards.

GC response factors were determined for the substrate and products by analyzing solutions with known concentrations. BHT impurity present in THF solvent was used also as an internal standard in the GC analysis.

Mass spectrometry allowed to compare the mass spectral patterns (m/z) of the reactions compounds. The most intense ions in the mass spectrum were (m/z): 97 and 126 for HMF, 128 and 97 for BHMF, 56 and 41 for DMTHF, 96 and 95 for DMF. Chromatograms and mass spectrum (GC–MS) for hydrogenation of HMF over 1%Ir/SiO_2(Cl) and acids are showed in the Supporting Information (Figs. S1 and S2).

The temperature of the GC injector was fixed at 513 K with the column detector at 533 K. The oven temperature was set at 363 K for 6 min followed by heating (10 K min^{-1}) up to 443 K and finally this temperature was keeping for 30 min. Specifically HMF (Sigma-Aldrich, ≥98%) and its hydrogenation products, BHMF (Santa Cruz Biotechnology, ≥98%), DMTHF (Sigma-Aldrich, ≥96%) and DMF (Sigma-Aldrich, ≥99%) were detected and quantified from the peaks with the retention time of 16.2, 10.8, 2.9 and 2.7 min respectively.

The rate constants have been obtaining from the slope (k') of log(1-X) versus time dependences, (where X is relative conversion up to until 35 min). The correspondent values were then calculated per metal surface atom according to:

$$\frac{(k'(\mathrm{min}^{-1}) \times HMF \quad concentration\ (\mathrm{mol.L}^{-1}) \times Total \quad number \quad of \quad iridium \quad atoms)}{(Dispersion \times Volume, \mathrm{L})} \tag{3}$$

where the total number of Ir atoms corresponds to the ratio between the metal loading (m_{Ir}) on the catalyst, the molar mass ($P_{M_{Ir}}$) and the Avogadro number (N_A): m_{Ir} x N_A/ $P_{M_{Ir}}$

3. Results

3.1. Catalyst characterization

Table 1 compiles the BET surface area, pore volume and pore size of the samples. SiO_2 exhibits a surface area of 293 $m^2 g^{-1}$. When the iridium species were introduced by impregnation in the silica support, its surface area, pore size and pore volume decreased. For instance 5%Ir/SiO_2 catalysts had a surface area of 284 $m^2 g^{-1}$ and pore volume of 0.706 $cm^3 g^{-1}$. The decrease in the surface area and pore volume after impregnation of the support by the iridium precursor solution may indicate a partial filling of the pores by iridium species. All samples display a typical IV isotherm with a H1 type hysteresis loop (Fig. 1). This kind of adsorption is characteristic of mesoporous materials with 2 D-hexagonal structure [40].

A diffraction pattern on a silica supported iridium catalysts (Fig. 2) consists of mixture of a highly dispersed iridium species particularly for 1%Ir/SiO_2. The silica support exhibit a broad peak in the 2θ range of 15°–30° which is assigned to the amorphous silica. Those assigned to metallic Ir are observed at 2θ = 40.7°, 47.3°, 69.1° and 83.4° for the reduced 3%Ir/SiO_2 and 5%Ir/SiO_2 samples. Diffraction peaks at 2θ = 28.0°, 34.7°, 40.1°and 54.0° assigned to IrO_2 that could be indexed to the standard diffraction data (JCPDS 15-0870) due to the rutile-type IrO_2 were not detected.

TEM of the iridium based catalysts is shown in Fig. 3. Fig. 3a shows that Ir nanoparticles in 1%Ir/SiO_2 catalyst are well dispersed on the support of SiO_2 and the average size of Ir is ca. 1.6 nm. For 3%Ir/SiO_2 catalyst (Fig. 3b) the average size of iridium nanoparticles was ca. 1.8 nm while for 5%Ir/SiO_2 the average iridium particle size was somewhat larger being 2.2 nm (Fig. 3c). These results suggest that as the iridium content increases the metal particle size increases. This is plausible since transition metals form only weak van der Waals interactions with the silica support [41].

A complementary study of 1%Ir/SiO_2 showing high angle annular dark field (HAADF) images obtained in STEM mode of the sample is presented in Fig. 4a. With this technique (Z-contrast) the Ir nanoparticles appear as bright dots over SiO_2 groundmass. The sample contains individual Ir nanoparticles having 1.8 ± 0.4 nm in diameter with a remarkably narrow size distribution in agreement with the TEM image (Fig. 3a).

Fig. 4b and c correspond to HAADF of the catalyst containing chlorine 1%Ir/SiO_2(Cl). Clearly, the distribution of Ir particles is quite

Table 1
N_2 physisorption of SiO_2 and iridium catalysts.

Sample	S_{BET} ($m^2 g^{-1}$)	Pore volume ($cm^3 g^{-1}$)	Pore diameter (nm)
SiO_2	293	0.789	10.9
1%Ir/SiO_2	295	0.801	9.7
3%Ir/SiO_2	294	0.747	9.6
5%Ir/SiO_2	284	0.706	9.7
1%Ir/SiO_2(Cl)	294	0.797	10.8

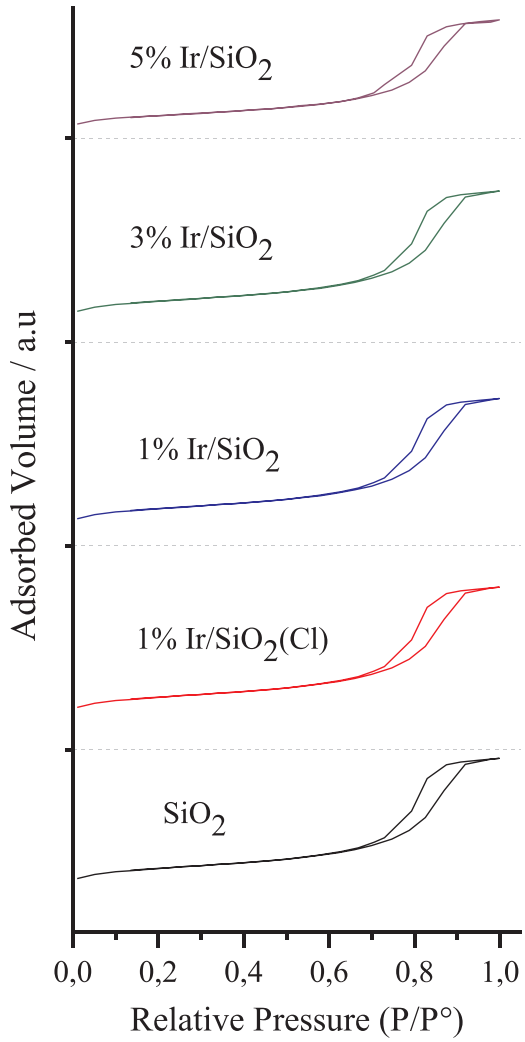

Fig. 1. N_2-physisorption of SiO_2 and supported iridium catalysts.

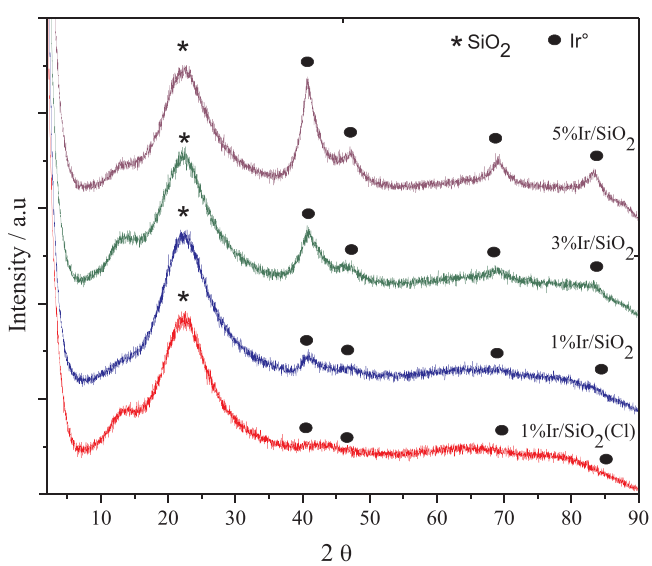

Fig. 2. XRD of iridium catalysts.

heterogeneous, with a mean particle size of 4.7 ± 2.8 nm. This value is considerably higher than that of the sample without Cl. Energy dispersive X-ray (EDS) analysis performed for individual Ir particles confirms the presence of Ir, while no signal attributable to chorine was detected. The EDS analysis corresponding to the particle inside the white square is given in Fig. 4b. On the contrary STEM-EDS performed over the bare support (Fig. 4b and c) of 1%Ir/SiO_2(Cl) indicated the presence of a minor amount of Cl and that the Ir particles in this case are larger and much more heterogeneous in size.

In addition, it can be seen that dispersion of iridium particles determined by TEM agrees well with the corresponding dispersion values obtained from chemisorption analysis especially for 1%Ir/SiO_2, 3%Ir/SiO_2 and 5%Ir/SiO_2 catalysts (Table 2). Noteworthy to remark that the presence of chlorine in 1%Ir/SiO_2(Cl) sample decreased the quantity of chemisorbed hydrogen to the lowest observed value (0.1 μmoL g_{cat}^{-1}) compared to other catalysts (Table 2). Heterogeneous and larger iridium particle for 1%Ir/SiO_2(Cl) are responsible for a decrease in the quantity of adsorbed hydrogen. It cannot be discarded that some adsorbed chlorine species on the iridium catalyst surface may block the active sites of the catalyst for hydrogen adsorption by forming a strong metal chlorine bond.

It must be added that a direct reduction in H_2 constitutes an efficient treatment to produce well dispersed iridium based catalysts prepared from organometallic precursors [42]. The direct reduction was chosen in the catalyst preparation done in present work instead of an oxidative treatment. The latter treatment may induce combustion of the organic ligands releasing too much heat and inducing thereby uncontrolled migration of iridium. In addition, oxidative treatment may generate iridium oxide species (IrO_2) which have a strong tendency to agglomerate forming large crystallites [42].

The distribution of iridium species before reduction may govern the iridium dispersion in the reduction step. The porous structure of the support may also play a strong role in the size and distribution of iridium particles especially when there are only weak interactions between the iridium precursor and silica substrate. The chemical nature of the support in general strongly affects interactions with metal particles. Weak interactions between SiO_2 and iridium species may not prevent diffusion and sintering of iridium species during activation process via reduction in hydrogen. In this work, this behavior can be minimized in synthesis of catalysts with small Ir particle sizes and high dispersion by direct reduction of the impregnated catalysts with H_2.

Removal of the solvent during drying may concentrate the impregnating solution to the point where crystallization of the metal precursor begins, forming a nucleus within the pores. Further drying may crystallize the iridium precursor in the amount related to the pore volume [43]. This feature may tentatively explain the fact that iridium dispersion is higher for low Ir loading as suggested by TEM analysis.

The most conclusive observation about the effect of the iridium precursor is in the metal dispersion. The 1%Ir/SiO_2(Cl) sample has particles much more heterogeneous in size compared with 1%Ir/SiO_2 sample. The reduction step may presumably promote removal of the cyclooctene ring of the iridium precursor by reduction and it may release HCl according to the previous work [44]. Halogen compounds are typically used to redisperse noble metal particles and numerous works have been published in this field [45]. Sintering and redispersion of supported metal particles are mainly governed by the balance between surface tension of supported particles and metal support interactions [46,47]. Chlorine species may be still bound to the surface after the reduction treatment. Residual chlorine species can be strongly bound to the surface of the metal species as confirmed by STEM-EDS analysis for 1%Ir/SiO_2(Cl) sample (Fig. 4b).

Fig. 5 shows NH_3-TPD profiles of the supported iridium catalysts (1%Ir/SiO_2, 1%Ir/SiO_2(Cl), 3%Ir/SiO_2 and 5%Ir/SiO_2). A very weak NH_3 desorption peak at a wide temperature range of 573–873 K is detected for 1%Ir/SiO_2, 3%Ir/SiO_2 and 5%Ir/SiO_2 catalysts. Generally, the strength of the acid sites, based on NH_3 desorption temperature, can be classified as weak (< 523 K), medium (523–673 K) and strong acid sites (above 673 K).

For 1%Ir/SiO_2(Cl) the amount of acid sites at both lower and higher NH_3-desorption temperature is higher (Fig. 5) in comparison with other

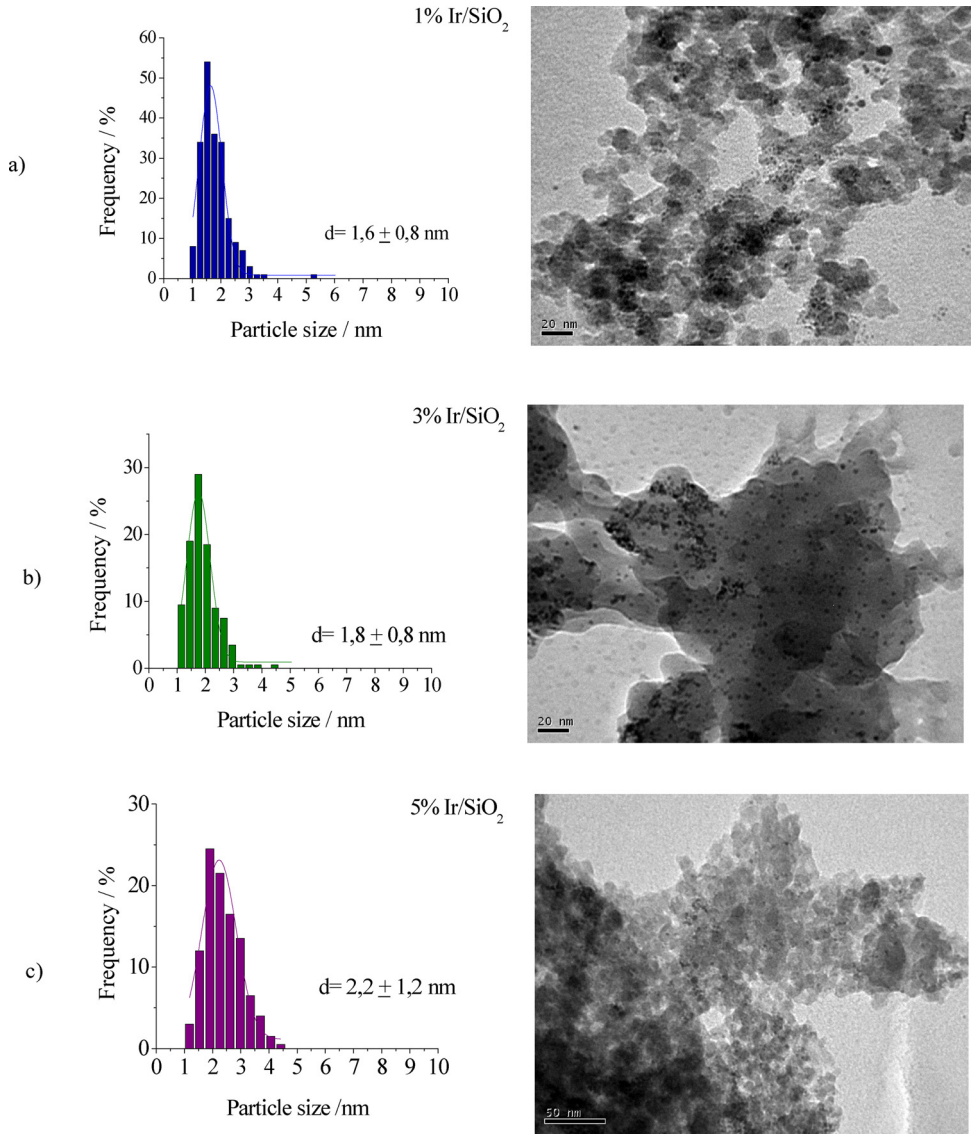

Fig. 3. Electron microscopy. Histograms and TEM images of a) 1%Ir/SiO_2, b) 3%Ir/SiO_2, and c) 5%Ir/SiO_2.

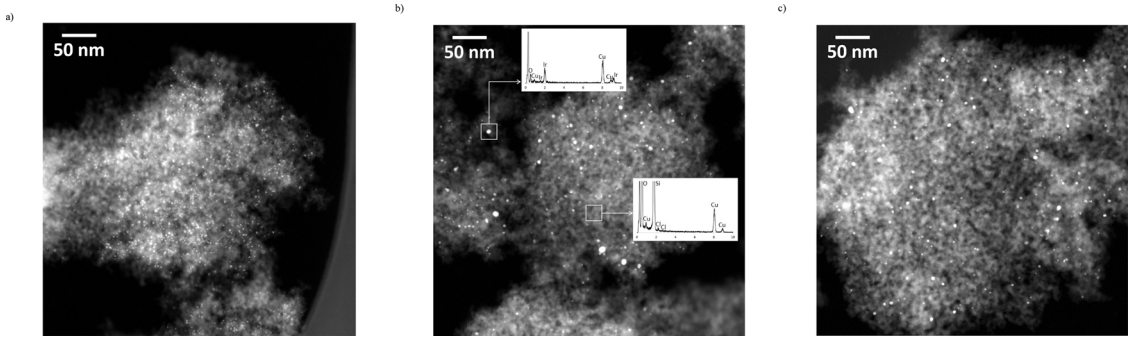

Fig. 4. High angle annular dark field (HAADF-STEM) images a) 1%Ir/SiO_2, b) 1%Ir/SiO_2(Cl) including EDS and c) 1%Ir/SiO_2(Cl).

catalysts. An increase in the total amount of the acid sites may be attributed to the presence of residual chlorine in 1%Ir/SiO_2(Cl) catalyst which was prepared by impregnation of the chlorine containing precursor. The quantification of the total amount of the acid sites (Table 3) revealed that the 1%Ir/SiO_2(Cl) catalyst presented the highest total quantity of acid sites with a value of 396 μmoL g_{cat}^{-1}.

H_2-TPR profile of 1%Ir/SiO_2 (Fig. 6) exhibits a hydrogen consumption peak at around 400 K due to the reduction of larger IrO_2 agglomerates. In addition, a second H_2 consumption peak is observed ca 490 K which may correspond to highly dispersed iridium species. It must be added that a minor H_2 consumption observed at temperatures higher than 600 K may be due to the presence of iridium species acting

Table 2
Metal particle size (d) and dispersion (D) determined by transmission electron microscopy and chemisorption results for iridium catalysts.

Sample	d_{TEM} (nm)	D_{TEM} (%)	D_{CHEM} (%)	Chemisorbed hydrogen (μmol g_{cat}^{-1})
1%Ir/SiO_2	1.6 ± 0.8	58[a,b]	50	13.1
3%Ir/SiO_2	1.8 ± 0.8	51[b]	38	32.4
5%Ir/SiO_2	2.2 ± 1.2	42[b]	28	37.1
1%Ir/SiO_2(Cl)	4.7 ± 2.8	20[a]	–[c]	0.1

[a] HAADF-STEM.
[b] TEM.
[c] Undetermined.

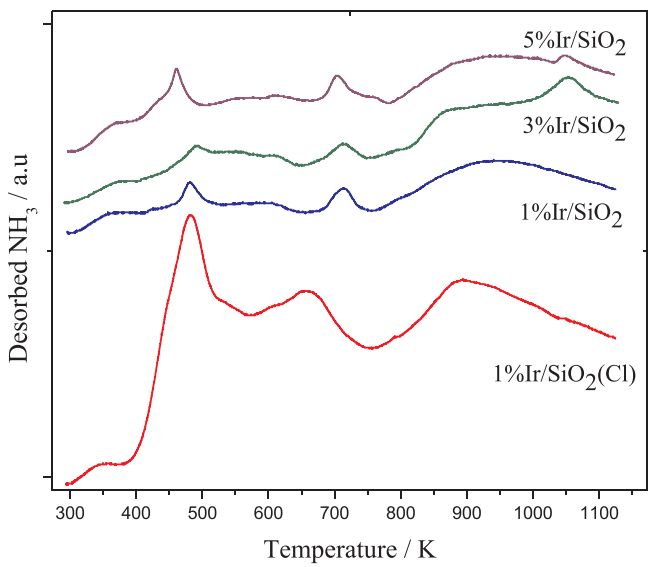

Fig. 5. NH_3-TPD analysis of the supported iridium catalysts.

Table 3
NH_3-TPD of the iridium catalysts.

Sample	NH_3 desorption (μmol g_{cat}^{-1})
1%Ir/SiO_2	94
3%Ir/SiO_2	109
5%Ir/SiO_2	117
1%Ir/SiO_2(Cl)	396

as anchoring sites at the interface of the metal nanoparticle with SiO_2 [48,49]. These iridium species are assigned to $Ir^{+}\delta$ cations in the interface between iridium and SiO_2 support. No reduction signals were seen in the H_2-TPR of SiO_2 alone. According to the previous work [50], hydrogen consumption of the lower reduction peak in general increases and shifts to a lower temperature with increasing Ir loading, while a higher reduction temperature peak almost does not change. It was observed that the presence of chlorine species delayed iridium reduction (Fig. 6). The total hydrogen consumption detected for 1%Ir/SiO_2(Cl), 1%Ir/SiO_2, 3%Ir/SiO_2 and 5%Ir/SiO_2 was respectively 122, 214, 521 and 682 μmol g_{cat}^{-1}.

The Ir4*f* core-level spectra of the iridium based catalysts are shown in Fig. 7. The presence of two different iridium species on the surface of the catalyst was evidenced by deconvolution of the Ir4*f* peaks. The two doublets (including $Ir4f_{5/2}$ and $Ir4f_{7/2}$) are identified as shown in Fig. 7. For 1%Ir/SiO_2 the binding energy (BE) corresponding to metallic iridium species in the orbital $4f_{7/2}$ is equal to 61.1 eV (Table 4) and in the orbital $4f_{5/2}$ the value of 63.6 eV was detected (Fig. 7a). In addition, the deconvoluted peaks indicated iridium oxide species attributed to the orbital $4f_{7/2}$ and $4f_{5/2}$ with BE of 62.8 eV and 65.8 respectively. The

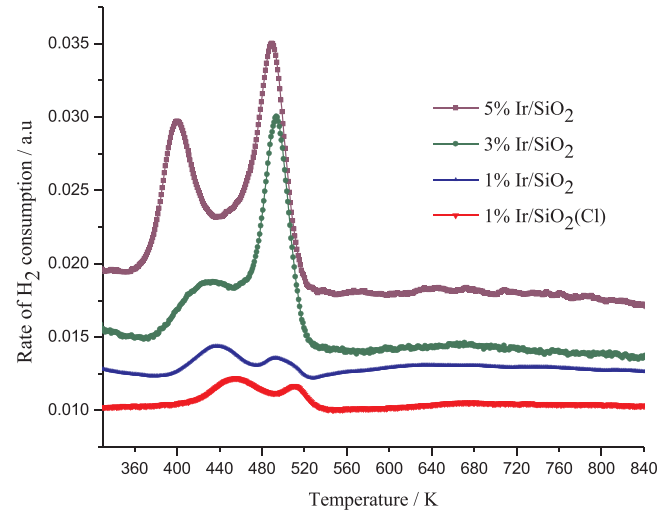

Fig. 6. TPR profiles of iridium based catalysts.

same results were observed for 3%Ir/SiO_2 and 5%Ir/SiO_2 catalysts (Fig. 7b and c). It must be added that the surface iridium metallic species content characterized by XPS increased with an increase of iridium loading in the catalyst. For instance, 1%Ir/SiO_2 exhibit 56% of metallic iridium species whereas for 3%Ir/SiO_2 76% of metallic iridium species were observed as shown Table 4. The doublets identified in all spectra can be assigned to the presence of surface metallic and oxide iridium species. In the case of 1%Ir/SiO_2(Cl) (Fig. 7d), more quantity of metallic Ir species were detected. Based on the XPS, traces of chlorine species were present as also evidenced by STEM-EDS (Fig. 4b). This reveals that after reduction at 723 K the chlorine species remain on the surface of the catalyst [45].

3.2. Catalytic tests with probe molecules (KP and EP)

The catalytic performance of the iridium catalysts was first investigated in the hydrogenation of ethyl pyruvate and ketopantolactone. These reactions provide an important synthetic approach to investigate catalytic activity in hydrogenation of the C=O bond. Synthesis of a large number of chemicals involves selective hydrogenation of α, β-unsaturated carbonyls into saturated compounds [51]. Hydrogenation of EP and KP produced ethyl lactate and pantolactone as products, respectively (Fig. 8). The aim to study these model compounds is also to obtain more knowledge concerned on the influence of some preparation parameters such as iridium precursor nature and the metal content (1, 3 and 5 wt.% of iridium) in the catalyst.

Fig. 8a and b show respectively the catalytic performance of the iridium based catalysts for hydrogenation of KP and EP. Activity of iridium catalysts in hydrogenation of these probe molecules is strongly influenced by the metal dispersion, defined as the ratio of Ir surface atoms to the total Ir atoms in the catalyst. To rationalize the factors influencing the reactivity and the product selectivity for each model compound the reaction rate constants (*k*) were calculated at 35 min of the reaction (Table 5). The *k* values were expressed per the total amount of iridium in the catalyst allowing to identify that the rate constant was dependent on the metal dispersion. It must be added that this behavior was observed for the catalysts prepared by a chlorine-free route (1%Ir/SiO_2, 3%Ir/SiO_2, 5%Ir/SiO_2).

A closer look must be given especially to 1%Ir/SiO_2(Cl) prepared from the chlorine-containing precursor. Supported VIII group metals are commonly prepared by impregnation of a support with chlorine containing precursors followed by thermal treatment. It has been reported that residual chlorine cannot be totally removed from the catalyst by conventional thermal treatments [42,45]. Therefore, it is of

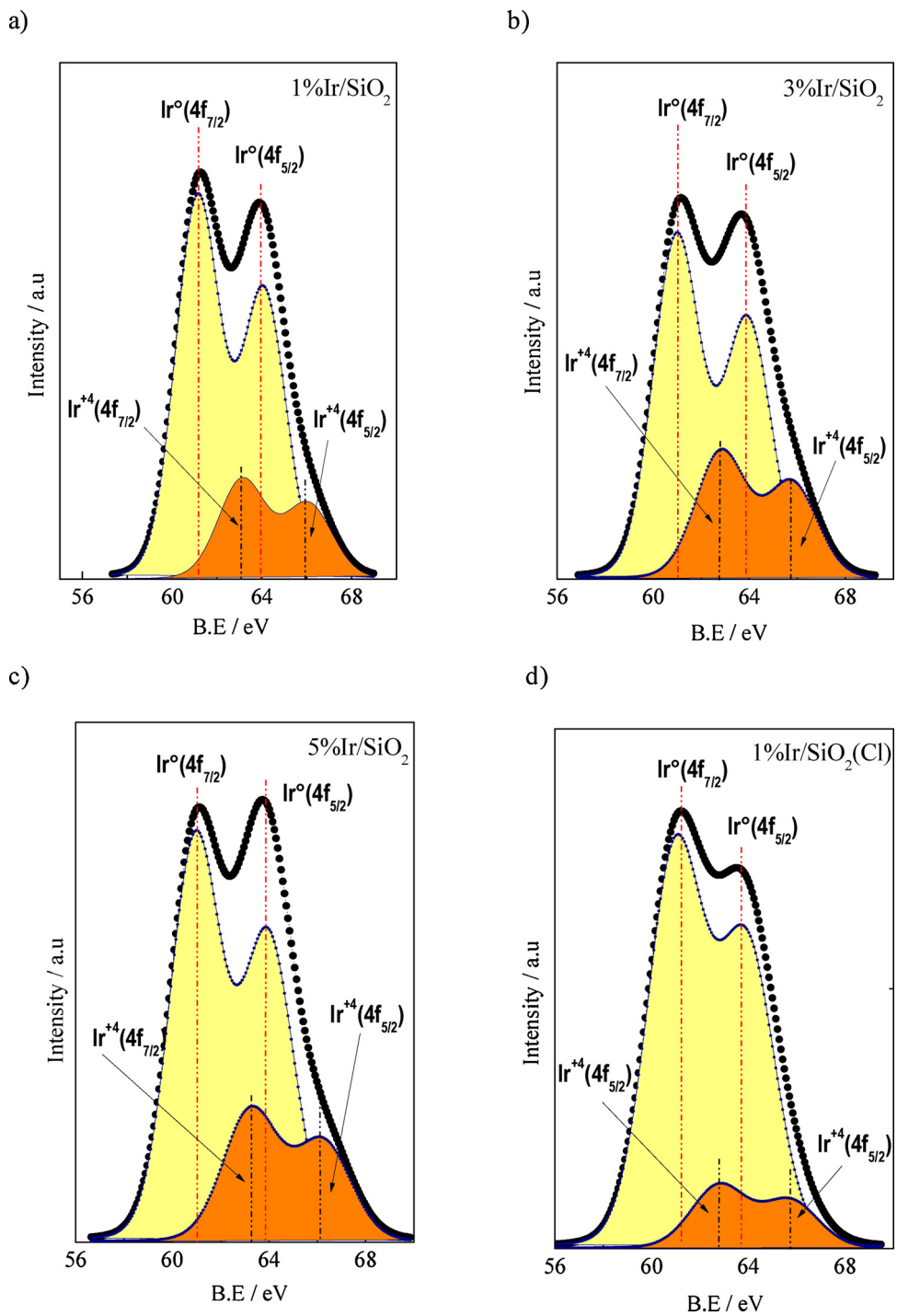

Fig. 7. XPS of the iridium catalysts.

interest to reveal a role of the residual chlorine species in catalysts prepared from a chlorine-containing precursor.

For both probe molecules a decrease in *k* values was noticed in the case of 1%Ir/SiO_2(Cl) catalyst compared with 1%Ir/SiO_2 (Table 5). For instance in hydrogenation of EP the rate constant 5.6 ($min^{-1}\,mol_{Ir}{}^{-1}\,mol$) for 1%Ir/$SiO_2$ is exceeding two fold the corresponding value for 1%Ir/SiO_2(Cl). A decrease in the hydrogenation activity of 1%Ir/SiO_2(Cl) for both probe molecules (KP and EP) may be attributed mainly to the iridium dispersion. The decrease in the hydrogenation activity for 1%Ir/SiO_2(Cl) of the probe molecules can be attributed the presence of larger iridium particles. To this effect it must be added that some residual chlorine can remain in the catalyst, not being decomposed during the catalyst pretreatment [45,52]. Chlorine species may act as a poison of the active iridium metal atoms required for hydrogenation [42,45,52] also explaining the observed decrease in its activity when compared with 1%Ir/SiO_2 catalyst. Thus activity decline for 1%Ir/SiO_2(Cl) (Table 5) can be due to a lower iridium dispersion, site blocking by chlorine species, electronic effects or a combination of them.

3.3. Hydrogenation of HMF to BHMF over Ir/SiO_2 catalysts

Selective hydrogenation of HMF was investigated over 1%Ir/SiO_2 and 1%Ir/SiO_2(Cl) showing much more promising behavior than

Table 4
Surface composition of the catalysts and binding energies (eV) of $Ir4f_{7/2}$.

Sample	Binding energy (eV)	% Atomic fractions
1%Ir/SiO_2	61.1[a]	56[a]
	62.8[b]	44[b]
3%Ir/SiO_2	61.0[a]	71[a]
	62.8[b]	29[b]
5%Ir/SiO_2	61.1[a]	76[a]
	62.9[b]	24[b]
1%Ir/SiO_2(Cl)	61.0[a]	86[a]
	62.8[b]	14[b]

[a] Iridium metallic.
[b] Oxide iridium species.

hydrogenation of the probe molecules (KP and EP). Striking differences in the performance of 1%Ir/SiO_2 and 1%Ir/SiO_2(Cl) in their ability to hydrogenate the probe molecules in comparison with HMF hydrogenation is observed. This point will be further addressed in the discussion part (*vide infra*).

Table 6 features the TOF numbers and the reaction rate constant k expressed per total amount of iridium in the catalyst. Similar TOF values measured at 10 min of the reaction were found in both cases indicating similar conversion at the beginning of the reaction, however a slight increase in activity was found for 1%Ir/SiO_2(Cl). It must be stressed that this catalyst exhibited the highest constant with the value of 4.5 ($min^{-1}\,mol_{Ir}^{-1}\,mol$). This sample also contains the largest quantity of total acid sites with a value of 396 μmoL g_{cat}^{-1} (Table 3). In the case of HMF chlorine species may act as active acid sites.

The main product obtained by hydrogenation of HMF with iridium based catalysts (1%Ir/SiO_2 and 1%Ir/SiO_2(Cl)) was BHMF (Scheme 2). In this case selectivity was 100% to BHMF and formation of MFA, which can be produced from deoxygenation of BHMF [15] or DMF and DMTHF was not observed. Our results are in agreement with the previous work [26], which reported for Ir/TiO_2 conversion of HMF equal to 99% and BHMF yield of 95% at 60 bar H_2 and 323 K.

3.4. Kinetics and modelling of HMF transformation to BHMF and DMF over Ir/SiO_2 catalysts in combination with H_2SO_4

The presence of sulfuric acid can enable one-pot synthesis of DMF from HMF over iridium based catalysts (Fig. 9a) and thus in this work kinetics in HMF transformation to BHMF and DMF was investigated in the presence of sulfuric acid using iridium based catalysts (1%Ir/SiO_2 and 1%Ir/SiO_2(Cl)) (Scheme 2).

TOF in HMF transformation with 1%Ir/SiO_2(Cl) and H_2SO_4 was twofold obtained in the absence of chlorine species (Table 7). It should, however, be noted that with the chlorine containing catalyst the HMF transformation rate was retarded after 230 min reaction time, whereas the catalyst without chlorine retained its activity in HMF transformation during the whole reaction time. On the other hand, higher conversion of HMF during 300 min was obtained in the absence of chlorine species.

Evolution of the products derived from HMF conversion in the presence of H_2SO_4 versus time using 1%Ir/SiO_2 and 1%Ir/SiO_2(Cl) catalysts can be observed in Fig. 9b and c, respectively. Particularly for the catalytic system comprising 1%Ir/SiO_2(Cl) and H_2SO_4 DMF and DMTHF were observed as products. When comparing selectivity at 70% conversion of HMF, it can be observed that Ir/SiO_2 + H_2SO_4 catalytic system was more selective towards BHMF, whereas DMF selectivity was higher in the presence of chorine containing Ir/SiO_2 with H_2SO_4 (Table 7). Noteworthy is also that despite catalyst deactivation and a lower rate for HMF transformation in the case of 1%Ir/SiO_2(Cl) with H_2SO_4, large amounts of an over-hydrogenolysis product, DMTHF with 23% selectivity at 70% conversion of HMF (Table 7) were formed. It has also been reported in the literature [26] that assistance of H_2SO_4 in HMF transformation is facilitating further transformation of BHMF to DMF. Furthermore, over-hydrogenolysis products such as DMTHF are usually promoted by strong acidic sites. Our results are in agreement with those obtained for one-pot hydrogenolysis of HMF to DMF [14]. The use of H_2SO_4 alone without the iridium catalyst in the reaction medium gave only DMF (Fig. 9a).

When plotting the concentration of DMF as a function of BMHF (Fig. 10a) it can be observed that DMF was formed faster over the chlorine containing catalyst. The ratio between the initial rates for formation of DMF and BMHF was 2.7 fold higher for chlorine containing catalyst than for the one without chlorine. Due to a slower rate observed for Ir/SiO_2, this catalyst could not catalyze over-hydrogenolysis of DMF to DMTHF (Fig. 10b), as was the case for chlorine containing Ir catalyst. The highest overall acidity of 1%Ir/SiO_2(Cl) catalyst (396 μmol g_{cat}^{-1}, Table 3) and the presence of H_2SO_4 may cause side reactions. It must be mentioned that in the catalytic tests in the presence of H_2SO_4, 1%Ir/SiO_2(Cl) exhibited a higher TOF and rate constant (Table 7) in comparison with 1%Ir/SiO_2 catalyst *per se* (Table 6). An increase in the initial activity with H_2SO_4 is due to additional formation of DMF as shown Fig. 9a. It must be added that Thananatthanachon et al. [29] reported that HMF in refluxing THF with formic acid and H_2SO_4 gave DMF in one-pot which is in agreement with our results. Again, it was not observed the presence of MFA. The previous studies suggest that hydrogenolysis of BHMF to DMF occurs via MFA as an intermediate [15]. It must be mentioned that hydrogenolysis products obtained by decarbonylation of HMF were also not detected under our experimental conditions.

Modeling of the experimental data from HMF transformation over Ir/SiO_2 together with H_2SO_4 for two types of precursors (with and without chlorine) was performed using Scheme 2 and the corresponding following rate equations:

$$r_{HMF\rightarrow BHMF} = k_1 C_{HMF}\, a \tag{4}$$

$$r_{BHMF\rightarrow DMF} = k_2 C_{BHMF}\, a \tag{5}$$

$$r_{DMF\rightarrow DMTHF} = k_3 C_{DMF}\, a \tag{6}$$

which should be solved together with the mass balances for different components in a batch reactor

$$-\frac{1}{\rho}\frac{dC_{HMF}}{dt} = r_{HMF\rightarrow BHMF};\quad \frac{1}{\rho}\frac{dC_{BHMF}}{dt} = r_{HMF\rightarrow BHMF} - r_{BHMF\rightarrow DMF};\quad \frac{1}{\rho}\frac{dC_{DMF}}{dt} = r_{BHMF\rightarrow DMF} - r_{DMF\rightarrow DMTMF};\quad \frac{1}{\rho}\frac{dC_{DMTMF}}{dt} = r_{DMF\rightarrow DMTHF} \tag{7}$$

where ρ is the catalyst bulk density, r_i and k_i are the rates and rate constants for respective steps, *etc*. In Eqs. (4)–(6) is a phenomenological activity function accounting for catalyst deactivation during the reaction with time t

$$a = a_0 e^{-k_d t} \tag{8}$$

where the initial activity a_0 was taken as unity. Such activity decline can originate from different reasons including product inhibition.

Thus, the model consisting of 4 fitted parameters was used to predict concentration dependences of 3 compounds. Kinetic modeling was performed using ModEst software [53]. The objective function (Q) for the residual sum of squares between the calculated and experimental data was minimized during the parameter estimation to search for the best-fit values using the Levenberg–Marquardt algorithm implemented in the software. The error function is defined as:

$$Q = \sum (C_{i,t\ (est)} - C_{i,t\ (exp)})^2 \tag{9}$$

where i and t denote the components and the corresponding times, respectively.

The accuracy of the model description was determined with the R^2 – coefficient or degree of explanation, which reflects comparison between

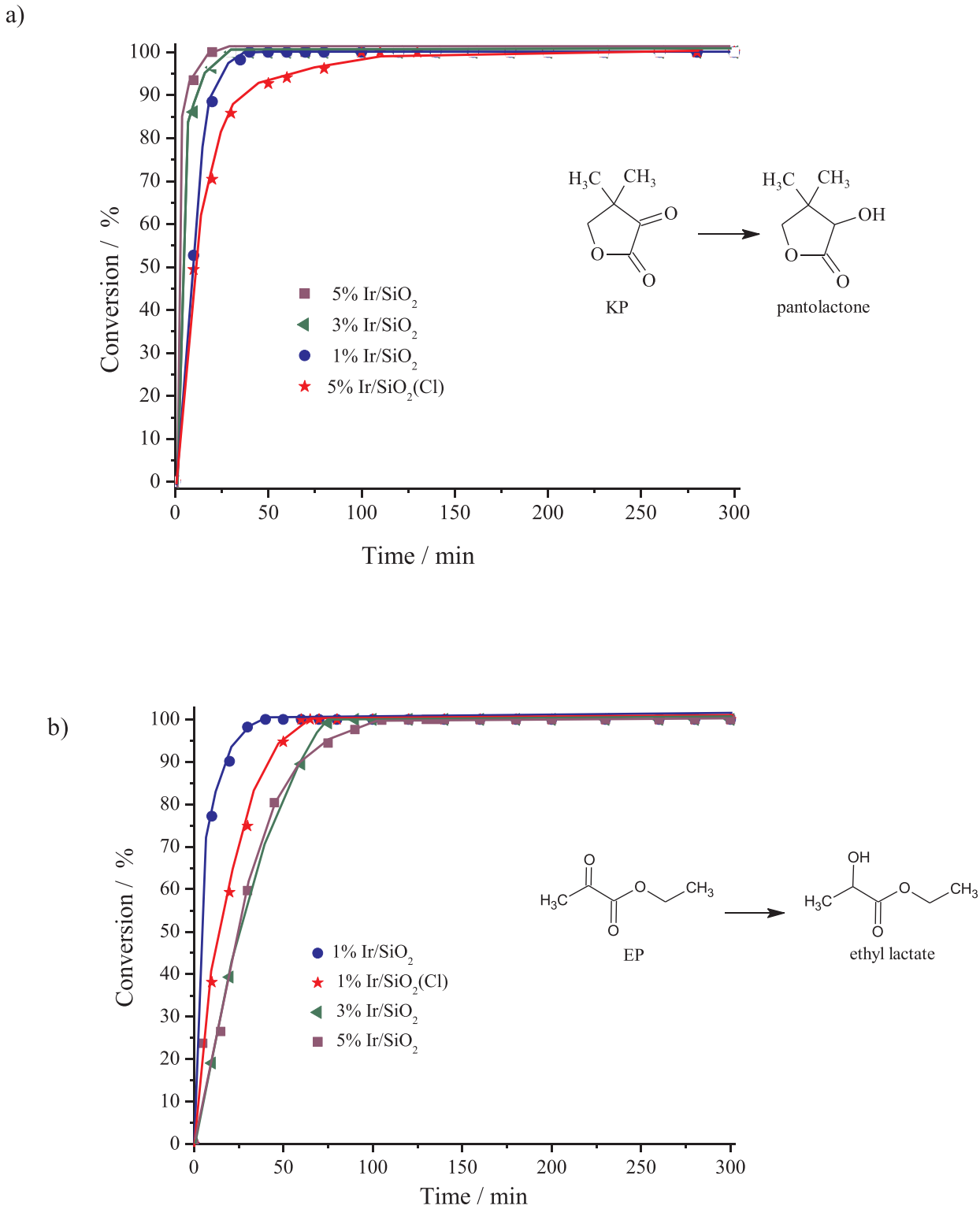

Fig. 8. Hydrogenation of probe molecules on Ir catalysts: a) KP and b) EP.

the residuals given by the model with the residuals of the simplest model, i.e. the average value of all data points. The R^2 value is given by expression:

$$R^2 = 100\frac{(y_{model}-y_{experiment})^2}{(y_{model}-\bar{y}_{experiment})^2} \quad (10)$$

Table 8 contains the values of lumped values of kinetic constants which include also the catalyst bulk density. The results presented in Fig. 9 clearly show that the model is able to capture the reaction network.

3.5. Recycling of Ir/SiO₂ catalyst

Finally recycling of the catalyst was studied in selective hydrogenation of HMF. In this case at the end of the first catalytic test 1%Ir/SiO_2 was re-used again without further activation for two more

Table 5
Reaction rate constant calculated until 35 min of reaction over iridium catalysts in the hydrogenation of ethyl pyruvate (EP) and ketopantolactone (KP) and dispersion determined by TEM and HAADF-STEM.

Catalyst	Dispersion (%)	k (min^{-1} mol_{Ir}^{-1} mol) (EP hydrogenation)	k (min^{-1} mol_{Ir}^{-1} mol) (KP hydrogenation)
1%Ir/SiO_2	58[a,b]	5.6	5.4
3%Ir/SiO_2	51[b]	1.6	2.5
5%Ir/SiO_2	42[b]	0.3	2.4
1%Ir/SiO_2(Cl)	20[a]	2.4	2.3

[a] HAADF-STEM.
[b] TEM.

Table 6
Catalytic performance in the HMF conversion over iridium catalysts (1%Ir/SiO_2, 1%Ir/SiO_2(Cl)).

Catalyst	Conversion (%)[a]	TOF (s^{-1})[b]	k (min^{-1} mol_{Ir}^{-1} mol)[c]	Selectivity[d]
1%Ir/SiO_2	60	0.5	0.24	100
1%Ir/SiO_2(Cl)	97	0.8	4.5	100

[a] Conversion determined at 300 min.
[b] Calculated after 10 min using the equation TOF = (initial moles of HMF × conversion)/(Ir moles × 600 s).
[c] Reaction rate constant calculated until 35 min of reaction.
[d] Selectivity to BHMF at 300 min.

consecutive catalytic tests at the same experimental conditions. Fig. 11 and Table 9 illustrate the catalytic performance of 1%Ir/SiO_2 catalyst during recycling. It must be stressed, that there was a decrease in catalytic activity probably due to deposition of residual organic species. These residual organic species suppress progressively the active sites responsible for hydrogenation of HMF. Previous studies have shown that furfural species have strong adsorption on metal base catalysts causing catalyst deactivation [54].

4. Discussion

Hydrogenation of ethyl pyruvate (EP) and ketopantolactone (KP) is generally considered as a structure sensitive reaction [55,56]. Small Pt particles have rendered high activity in ethyl pyruvate reaction [57]. In the current work hydrogenation of EP and KP was used to evaluate the effect of iridium dispersion on the C=O hydrogenation. The activity of iridium catalysts in hydrogenation of EP and KP was clearly influenced by the metal dispersion. Based on the results for 1%Ir/SiO_2, 3%Ir/SiO_2 and 5%Ir/SiO_2 catalysts (Table 5) it can be noticed that the reaction rate constants decrease when the dispersion decreases. Subsequently, 1%Ir/SiO_2 which exhibited the highest rate constant was selected for further investigation of HMF hydrogenation. As comparison 1%Ir/SiO_2(Cl) was also evaluated in HMF hydrogenation to elucidate the role of the residual chloride.

It must be added that iridium was selected to be investigated as an active metal in this study due to high activity and selectivity reported in the literature [16,20,26,27] and as a choice to avoid leaching and increase the catalyst stability [58]. A conclusive indication for the effect of the type of metal on hydrogenation of HMF is reported elsewhere where the authors have demonstrated that iridium exhibited better performance than other metals such as Pd and Ni [58,59]. This previous work reported a TOF value of 300 h^{-1} which is close to TOF value for 1%Ir/SiO_2 catalyst (Table 6) of our study as already mentioned.

Catalytic performance in hydrogenation of the probe molecules (EP and KP) with iridium catalysts (1%Ir/SiO_2; 3%Ir/SiO_2; 5%Ir/SiO_2) can be explained based on the metal dispersion. This is clearly seen in the catalytic results presented in Table 5. The *k* values decrease markedly as the metal dispersion decreases. This is in agreement with the conclusions reported by previous work [57]. The effect of the residual chlorine species in 1%Ir/SiO_2(Cl) catalyst must be also considered. This catalyst exhibited a *k* value lower in comparison with the corresponding value for 1%Ir/SiO_2. This result can be attributed not only to a lower iridium dispersion but also to some suppression of the iridium active sites by chlorine species. This possibility cannot be ruled out since traces of chlorine species were detected by XPS and STEM-EDS for 1%Ir/

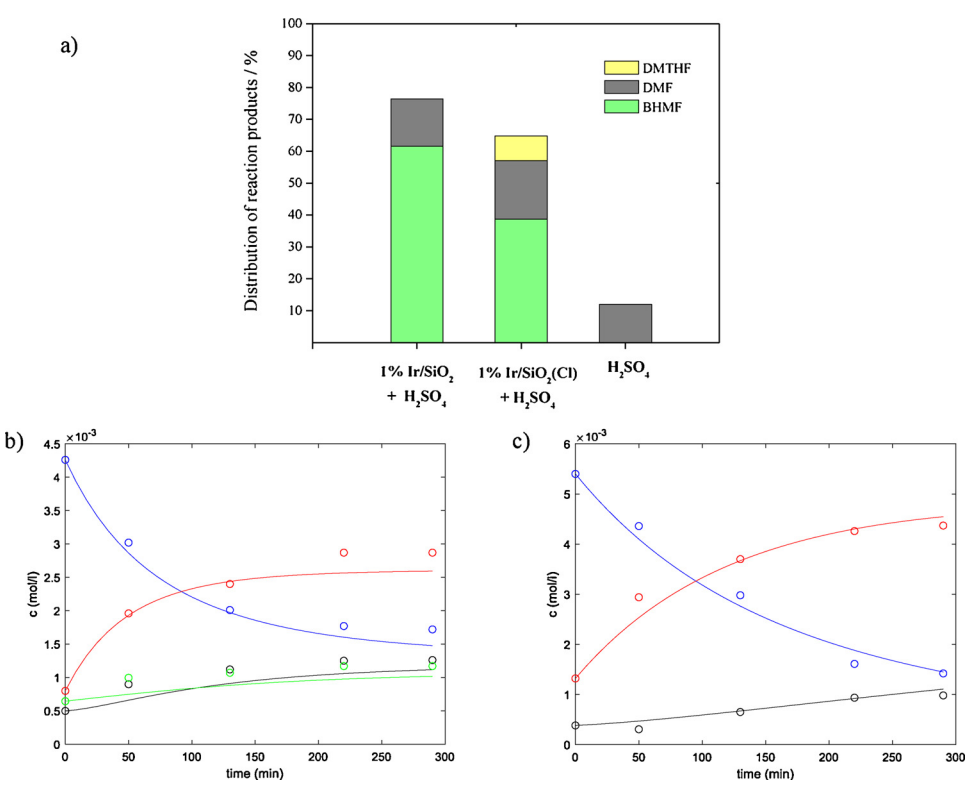

Fig. 9. Hydrodeoxygenation of HMF in the presence of sulfuric acid. a) Distribution of products after 300 min, as well as concentration profiles over b) 1%Ir/SiO_2 and c) 1%Ir/SiO_2(Cl). Experiment (O), model (-), blue HMF, red BHMF, black DMF, green DMTHF. (For interpretation of the references to colour in this figure legend, the reader is referred to the web version of this article).

Table 7
Catalytic performance of 1%Ir/SiO_2, 1%Ir/SiO_2(Cl) in the presence of sulfuric acid.

Catalysts	Conversion (%)[a]	TOF (s^{-1})[b]	k (min^{-1} mol_{Ir}^{-1} mol)[c]	Selectivity to BHMF[d]	Selectivity to DMF[d]	Selectivity to DMTHF[d]
1%Ir/SiO_2 + H_2SO_4	78	3.0	2.0	83	17	0
1%Ir/SiO_2(Cl) + H_2SO_4	74	5.9	4.6	52	24	23

[a] Conversion determined at 300 min.
[b] Calculated after 10 min using the equation TOF = (initial moles of HMF × conversion)/(Ir moles × 600 s).
[c] Reaction rate constant calculated until 35 min of reaction.
[d] Selectivity at 70% conversion (%).

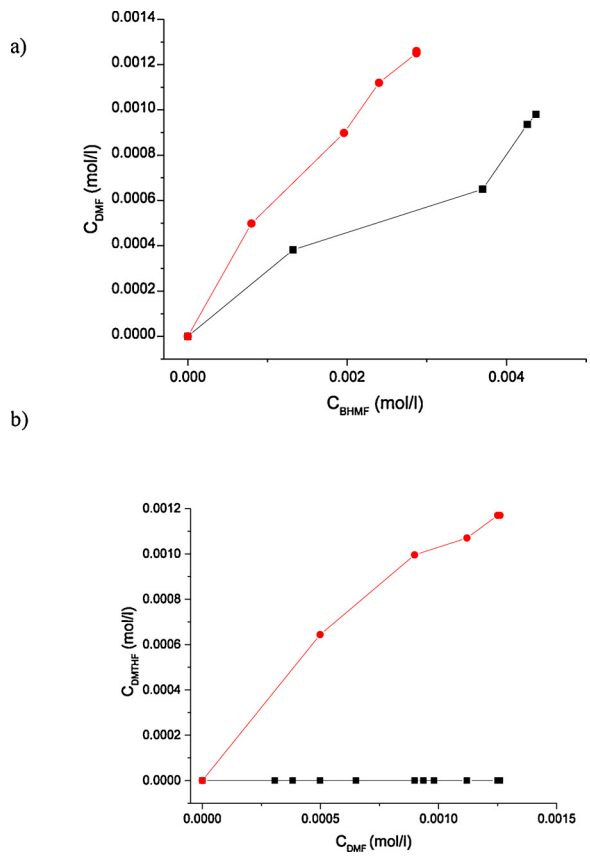

Fig. 10. Concentration of a) DMF as a function of BHMF concentration and b) concentration of DMTHF as a function of DMF concentration. Notation: 1%Ir/SiO_2 + H_2SO_4 (●) and 1%Ir/SiO_2(Cl) + H_2SO_4 (■).

SiO_2(Cl). Chemisorption results for 1%Ir/SiO_2(Cl) (Table 2) confirm presence of larger iridium particles and more heterogeneity in size distribution than in the case of 1%Ir/SiO_2 catalyst. In this respect, only a residual fraction of accessible iridium atoms of 1%Ir/SiO_2(Cl) may be involved in hydrogenation of the probe molecules. It must be added that for the probe molecules oxygen in the carbon-oxygen bond of the carbonyl group attracts electrons. However, in the presence of adjacent electron-attracting groups the carbonyl group may be destabilized compromising some polarization of these molecules on the catalyst surface.

Regarding HMF, let us first consider its hydrogenation over iridium based catalysts without H_2SO_4 in the reaction medium. Multiple reactions could take place during hydrogenation of HMF, including hydrogenation of the carbonyl group of furan ring, removal of carbonyl or carboxyl group and ring opening of furan. HMF is first hydrogenated to BHMF which can further deoxygenated to MFA and finally deoxygenated to DMF [15]. In the experimental conditions of the current work the main product obtained by hydrogenation of HMF with iridium based catalysts (1%Ir/SiO_2 and 1%Ir/SiO_2(Cl)) was BHMF. Formation of MFA which can be produced from deoxygenation of BHMF [15] was not observed.

Different factors can be tentatively proposed to interpret preferential hydrogenation of the C═O bond in HMF over Ir/SiO_2 by the presence of chlorine species. A fundamental question is why chlorine species enhance the selective hydrogenation of HMF. Selectivity to BHMF can be improved by inhibiting hydrogenation of the C═C bond. Knowledge of hydrogenation rates of C═C and C═O bonds is helpful to interpret selectivity changes that may occur in hydrogenation of multifunctional compounds [25]. For HMF hydrogenation, the acid sites can activate the hydrogenation of the C═O bond according to the literature [60]. Surface acidity of iridium catalysts measured by ammonia TPD (Fig. 5 and Table 3) suggests that the catalyst prepared with a chlorine-containing precursor (1%Ir/SiO_2(Cl)) has a higher total acidity (Table 3). Chlorine species on the catalyst surface (confirmed by XPS and STEM-EDS analysis) may induce some polarization of the carbonyl group of HMF promoting its adsorption. The presence of chlorine species may lead to a certain amount of electron deficient iridium species even after reduction of the catalyst. This may promote the local electronic density around the iridium species influencing the stability and reactivity of HMF. Thus, a lower dispersion of 1%Ir/SiO_2(Cl) is counterbalanced by the presence of chlorine species. In this respect, it should be considered that in hydrogenation of HMF, chlorine species activate the C═O group facilitating hydrogen transfer from the adjacent iridium atoms to the oxygen atom of the C═O bond. The same singularity was is in agreement with the conclusion drawn by previous work [60], where it is suggested that Lewis sites promotes the adsorption and activation of the C═O group of HMF via the lone pair of oxygen. It must be also considered, that some resonance stabilization especially in HMF ring may compensate some destabilization promoted by the adjacent groups of the carbonyl group. As a result, HMF must be a better electron donor than the probe molecules (KP and EP). Moreover, HMF may adsorb more strongly promoting hydrogenation of the C═O bond [61]. On the other hand, it must be also taken into account that the presence of π-system in HMF may enhance its interactions with the catalyst surface. Such interactions between the metal surface and oxygen in the HMF carbonyl group yielding BHMF would be allowed by a preferential adsorption in the η^1(O) configuration as suggested by the previous work

Table 8
Values of parameters for the model comprising Eqs. (4)–(8).

catalyst/Parameter	$\rho k_1 min^{-1}$	$\rho k_2 min^{-1}$	$\rho k_3 min^{-1}$	$k_d min-1$	R^2, %
1%Ir/SiO_2 + H_2SO_4	0.0057 ± 0.0005	0.00093 ± 0.00015	negligible	0.0017 ± 0.001	99.01
1%Ir/SiO_2(Cl) + H_2SO_4	0.0097 ± 0.0016	0.0045 ± 0.001	0.0045 ± 0.0016	0.0083 ± 0.0024	92.43

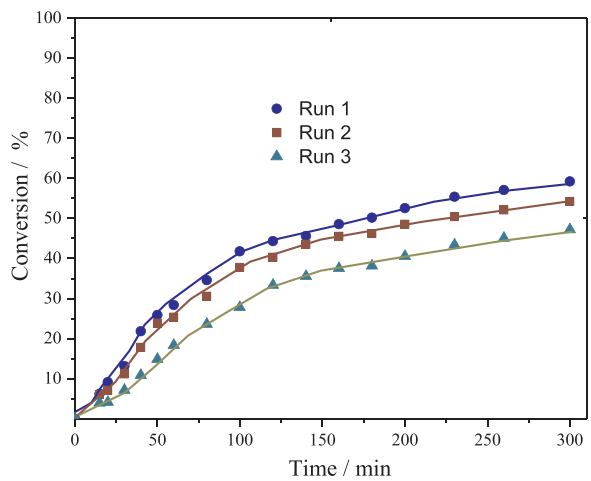

Fig. 11. Concentration profiles for recycling experiments with 1%Ir/SiO_2 catalyst.

Table 9
Catalytic performance of the 1%Ir/SiO_2 catalyst in the reuse in the HMF transformation.

Reaction	Conversion (%)[a]	k (min^{-1} mol_{Ir}^{-1} mol)[b]
0	60	0.24
Recycle 1	54	0.21
Recycle 2	47	0.14

[a] Conversion determined at 300 min.
[b] Reaction rate constant calculated until 35 min of reaction, respectively.

[62]. Finally, some influence of iridium oxide species as an important catalytic descriptor cannot be discarded. The presence of these species can also influence hydrogenolysis of BHMF to DMF. Table 4 presents the XPS results of iridium catalysts indicating existence of iridium oxide on the catalyst. Iridium oxidized species, in contact or in the vicinity of metallic iridium may act as Lewis sites, interacting with the lone electron pair of oxygen atom of the C=O group favoring its hydrogenation [62]. The promotion effect of metal oxide species in the adsorption of the substrate at the C=O bond is well supported by early work [16].

Applicability of H_2SO_4 to assist hydrodeoxygenation of BHMF obtained from hydrogenation of HMF (Scheme 2) was elucidated in this work. The presence of sulfuric acid can enable one-pot synthesis of DMF from HMF over iridium based catalysts. For the combination of sulfuric acid with 1%Ir/SiO_2(Cl) DMTHF was also observed as a product (Fig. 9). In addition, it must be stressed that 1%Ir/SiO_2(Cl) exhibits the highest total acidity (Table 3) when compared with other iridium catalysts.

A drawback of using strong acids is associated with possible side reactions [39]. Heterogeneous catalysts can be deactivated when used or recycled over a long period of time due to deposition of heavy by-products on the surface of the catalyst or leaching of the active sites from the catalyst surface [63]. Traditionally, mineral acids such as H_2SO_4 are used as homogeneous catalysts in manufacturing of the high value-added chemicals. However, homogeneous mineral acids such as H_2SO_4 have been reported to promote leaching of components into the reaction medium. It must be, therefore, mentioned that a decrease in the observed activity for iridium catalysts may be due to both deposition of by-products and the corrosive effect of H_2SO_4.

Combination of iridium catalysts and H_2SO_4 can be viewed as an effective strategy to convert HMF to DMF in one-pot. The role of H_2SO_4 as Brönsted acid is in assisting dehydroxylation in the presence of hydrogen giving BHMF and water. Importantly, for the combination of 1% Ir/SiO_2(Cl) and H_2SO_4, DMTHF was also observed as a product (Fig. 9). The presence of acid sites in the 1%Ir/SiO_2(Cl) and H_2SO_4 catalytic system may be responsible for such behavior [14].

5. Conclusions

Selective hydrogenation of biomass derived 5-hydroxymethylfurfural, an important platform molecule for production of value added compounds, was investigated over iridium based catalysts. Two probe molecules, EP and KP, were evaluated as an approach to investigate specifically the capability of iridium selectively hydrogenate the C=O bond.

The effect of the iridium precursor and addition of a mineral acid such as H_2SO_4 was evaluated in the catalytic transformation of HMF.

For 1%Ir/SiO_2(Cl) catalyst prepared with the chlorine containing iridium precursor the highest total acidity was observed. The presence of chlorine species as a source of acid sites was crucial for activation of the carbonyl group in HMF promoting formation of BHMF.

A mineral acid (H_2SO_4) as a source of Brönsted acid sites together with the iridium based catalyst was highly effective in one-pot chemical transformation of HMF to DMF.

Acknowledgments

The authors are grateful to FONDECYT1161660 and FONDECYT1180243 for the financial support. J. Llorca is a Serra Hunter Fellow and is grateful to ICREA Academia program and grant GC 2017 SGR 128.

Appendix A. Supplementary data

Supplementary material related to this article can be found, in the online version, at doi:https://doi.org/10.1016/j.apcatb.2018.09.026.

References

[1] J.N. Chheda, Y. Roman-Leshkov, J.A. Dumesic, Production of 5-hydroxymethtlfurfural and furfural by dehydration of biomass-derived mono- and polysaccharides, Green Chem. 9 (2007) 342–350.
[2] Z. Xu, P. Yan, W. Xu, X. Liu, Z. Xia, B. Chung, S. Jia, Z.C. Zang, Hydrogenation/hydrolytic ring opening of 5-HMF by cp*-iridium (III) half-sandwich complexes for bioketones synthesis, ACS Catal. 5 (2015) 788–792.
[3] J.P. Lange, Lignocellulose conversion: an introduction, Biofuels Bioprod. Biorefin. 1 (2007) 39–48.
[4] A. Corma, S. Iborra, A. Velty, Chemical routes for the transformation of biomass into chemicals, Chem. Rev. 107 (6) (2007) 2411–2502.
[5] J.N. Chheda, G.W. Huber, J.A. Dumesic, Liquid-phase catalytic processing of biomass-derived oxygenated hydrocarbons to fuels and chemicals, Angew. Chem. Int. Ed. 46 (38) (2007) 7164–7183.
[6] E.L. Kunkes, D.A. Simonetti, R.M. West, J.C.S. Ruiz, C.A. Gartner, J.A. Dumesic, Catalytic conversion of biomass to monofunctional hydrocarbons and target liquid-fuel classes, Science 322 (2008) 417–421.
[7] P. Lanzafame, D.M. Temi, S. Perathoner, G. Centi, A. Macario, A. Aloise, G. Giordano, Etherification of 5-hydroxymethyl-2-furfural (HMF) with ethanol to biobased components using mesoporous solid acid catalysts, Catal. Today 175 (2011) 435–441.
[8] L. Cottier, G. Descotes, 5-hydroxymethylfurfural syntheses and chemical transformations, Trends Heterocycl. Chem. 2 (1991) 233–248.
[9] M.R. Grochowski, W. Yang, A. Sen, Mechanistic study of a one-step catalytic conversion of fructose to 2,5-dimethyltetrahydrofuran, Chem. Eur. J. 18 (2012) 12363–12371.
[10] M. Mascal, S. Dutta, Chemical-catalytic approaches to the production of furfurals and levulinates from biomass, Top. Curr. Chem. 353 (2014) 41–83.
[11] T.B. Rauchfuss, T. Thananatthanachon, Efficient Method for Preparing 2,5-Dimethylfuran, US 8 324 409 B2, (2012).
[12] Y.B. Huang, M.Y. Chen, L. Yan, Q.X. Guo, Y. Fu, Nickel-tungsten carbide catalysts for the production of 2,5dimethylfuran from biomass-derived molecules, ChemSusChem 7 (2014) 1068–1072.
[13] Y. Roman, C. Barret, Z. Liu, J. Dumesic, Production of dimethylfuran for liquids fuels from biomass-derived carbohydrates, Nature 447 (2007) 982–985.
[14] S. Srivastava, G.C. Jadeja, J. Parikh, Influence of supports for selective production of 2,5-dimethylfuran via bimetallic copper-cobalt catalyzed 5-hydroxymethylfurfural hydrogenolysis, Chin. J. Catal. 38 (2017) 699–709.
[15] P. Yang, Q. Cui, Y. Zu, X. Liu, G. Lu, Y. Wang, Catalytic production of 2,5-dimethylfuran from 5-hydroxymethylfurfural over Ni/Co_3O_4 catalyst, Catal. Commun. 66 (2015) 55–59.

[16] Y. Nakagawa, K. Takada, M. Tamura, K. Tomishige, Catalytic reduction of biomass-derived furanic compounds with hydrogen, ACS Catal. 3 (2013) 2655–2668.
[17] F. Delbecq, P. Sautet, Competitive C=C and C=O adsorption of α-β-unsaturated aldehydes on Pt and Pd surfaces in relation with the selectivity of hydrogenation reactions: a theoretical approach, J. Catal. 152 (1995) 217–236.
[18] Y. Wang, X. Tong, Y. Yan, S. Xue, Y. Zhang, Efficient and selective conversion of hexose to 5-hydroxymethylfurfural with tin-zirconium containing heterogeneous catalysis, Catal. Commun. 50 (2014) 38–43.
[19] N. Shi, Q. Liu, Q. Zhang, T. Wang, L. Ma, High yield production of 5-hydroxymethylfurfural from cellulose by high concentration of sulfates in biphasic system, Green Chem. 15 (2013) 1967–1974.
[20] G. Guan, D.D. Zhang, Y. Pan, M. Iguchi, M.J. Ajitha, J. Hu, H. Li, C. Yao, M.H. Huang, S. Min, J. Zheng, Y. Himeda, H. Kawanami, K.W. Huang, Dehydrogenation of formic acid catalyzed by a ruthenium complex and *N*, *N*,-diimine ligand, Inorg. Chem. 56 (2017) 438–445.
[21] R.J. van Putten, J.C. van der Waals, E. de Jong, C.B. Rasrendra, H.J. Heeres, J.G. de Vries, Hydroxymethylfurfural, a versatile platform chemical made from renewable resources, Chem. Rev. 113 (2013) 1499–1597.
[22] S. Nishimura, N. Ikeda, K. Ebitani, Selective hydrogenation of biomass-derived 5-hydroxymethylfurfural (HMF) to 2,5-dimethylfuran (DMF) under atmospheric hydrogen pressure over carbon supported PdAu bimetallic catalyst, Catal. Today 232 (2014) 89–98.
[23] Y. Zu, P. Yang, J. Wang, X. Liu, J. Ren, G. Lu, Y. Wang, Efficient production of the liquid fuel 2,5-dimethylfurfural over Ru/Co_3O_4 catalyst, Appl. Catal. B 146 (2014) 244–248.
[24] A.S. Nagpure, N. Lucas, S.V. Chilukuri, Efficient preparation of liquid fuel 2,5 dimethylfuran from biomass-derived 5-hydroxymethylfurfural over Ru-NaY catalyst, ACS Sustain. Chem. Eng. 3 (2015) 2909–2916.
[25] X. Tang, J. Wei, N. Ding, Y. Sun, X. Zeng, L. Hu, S. Liu, T. Lei, L. Lin, Chemoselective hydrogenation of biomass derived 5-hydroxymethylfurfural to diols: key intermediates for sustainable chemicals, materials and fuels, Renew. Sustain. Energy Rev. 77 (2017) 287–296.
[26] H. Cai, C. Li, A. Wang, T. Zhang, Biomass into chemicals: one pot production of furan-based diols from carbohydrates via tandem reactions, Catal. Today 234 (2014) 59–65.
[27] M. Tamura, K. Tokonami, Y. Nakagawa, K. Tomishige, Rapid synthesis of unsaturated alcohols under mild conditions by highly selective hydrogenation, ChemComm 49 (2013) 7034–7036.
[28] T. Thananatthanachon, T.B. Rauchfuss, Efficient route to hydroxymethylfurans from sugars via transfer hydrogenation, ChemSusChem 3 (2010) 1139–1141.
[29] T. Thananatthanachon, T.B. Rauchfuss, Efficient production of the liquid fuel 2,5-dimethylfuran from fructose using formic acid as a reagent, Angew. Chem. Int. Ed. 49 (2010) 6616–6618.
[30] G. Balme, E. Bossharth, N. Monteiro, Pd assisted multicomponent synthesis of heterocycles, Eur. J. Org. Chem. 21 (2003) 4101–4111.
[31] M. Akizuki, Y. Oshima, Kinetics of glycerol dehydration with WO_3/TiO_2 in supercritical water, Ind. Eng. Chem. Res. 51 (2012) 12253–12257.
[32] A. Corma, G. Huber, L. Sauvanaud, P. Oconnor, Biomass to chemicals: catalytic conversion of glycerol/water mixtures into acrolein, reaction network, J. Catal. 257 (2008) 163–171.
[33] B. Peng, C. Zhao, I. Mejía-Centeno, G.A. Fuentes, A. Jentys, J.A. Lercher, Comparison of kinetics and reaction pathways for hydrodeoxygenation of C_3 alcohols on Pt/Al_2O, Catal. Today 183 (2012) 3–9.
[34] N. Nikbin, S. Caratzoulas, D.G. Vlachos, On the Brönsted acid-catalyzed homogeneous hydrolysis of furans, ChemSusChem 6 (2013) 2066–2068.
[35] N.W. Cant, L.H. Little, Lewis and Brönsted acid sites on silica-alumina, Nature 211 (1966) 69–70.
[36] H. Takagi, T. Isoda, K. Kusakabe, S. Morooka, Effects of solvents on the hydrogenation of mono-aromatic compounds using noble-metal catalysts, Energy Fuels 13 (1999) 1191–1196.
[37] G.C. Luijkx, N.P. Huck, F. van Rantwijk, L. Maat, H. van Bekkum, Ether formation in the hydrogenolysis of hydroxymethylfurfural over palladium catalysts in alcoholic solution, Heterocycles 77 (2009) 1037–1044.
[38] J.T. Wehrli, A. Baiker, D.M. Monti, H.U. Blaser, Particle size effect on enantioselective hydrogenation of ethyl pyruvate over alumina-supported platinum catalyst, J. Mol. Catal. 49 (1989) 195–203.
[39] L. Bui, H. Luo, W.R. Gunther, Y. Roman-Leshkov, Domino reaction catalyzed by zeolites with Brönsted and Lewis acid sites for the production of γ-valerolactone from furfural, Angew. Chem. Int. Ed. 52 (2013) 8022–8025.
[40] D. Zhao, Q. Huo, J. Feng, B.F. Chmelka, G.D. Stucky, Nonionic triblock and star diblock copolymer and oligomeric surfactant synthesis of highly ordered, hydrothermally stable, mesoporous silica structures, J. Am. Chem. Soc. 120 (1998) 6024–6036.
[41] R. Lamber, N. Jaeger, G. Schulz-Ekloff, Microstructure resulting from metal-support interactions on heterogeneous catalysts, Chem. Ing. Tech. 63 (1991) 681–691.
[42] S. Kaneko, M. Izuka, A. Takahashi, M. Ohshima, H. Kurokawa, H. Miura, Pt dispersion control in Pt/SiO_2 by calcination temperature using chloroplatinic acid as catalyst precursor, Appl. Catal. A: Gen. 427 (428) (2012) 85–91.
[43] I.V. Yentekakis, R.M. Lambert, M. Konsolakis, N.K. Kontos, On the effects of residual chloride and of barium promotion on $Pt/\gamma\text{-}Al_2O_3$ catalysts in the reduction of NO by propene, Catal. Lett. 81 (2002) 181–185.
[44] M.T. Atlay, M. Preece, G. Strukul, B.R. James, Selective, catalytic oxidation using hydrogen/oxygen mixtures with solutions of iridium and rhodium complexes, Can. J. Chem. 61 (1983) 1332–1338.
[45] J.H. Sinfelt, G.H. Via, Dispersion and structure of platinum-iridium catalysts, J. Catal. 56 (1979) 1–11.
[46] J. Lif, M. Skoglundh, L. Löwendahl, Stabilising alumina supported nickel particles against sintering in ammonia/hydrogen atmosphere, Appl. Catal. A.: Gen. 274 (2004) 61–69.
[47] F. Lonyi, J. Valyon, On the interpretation of the NH_3-TPD patterns of H-ZSM-5 and H-mordenite, Microporous Mesoporous Mater. 47 (2001) 293–301.
[48] G. Borda, H. Rojas, J. Murcia, J.L.G. Fierro, P. Reyes, M. Oportus, Hydrogenation of citral on Ir/SiO_2 catalysts. Effect of the addition of Nb_2O_5 on surface and catalytic properties, React. Kinet. Catal. Lett. 92 (2007) 369–376.
[49] H.F.J. van't Blik, J.B.A.D. van Zon, T. Huizinga, J.C. Vis, D.C. Koningsberger, R. Prins, An extended x-ray absorption fine structure spectroscopy study of a highly dispersed rhodium/aluminum oxide catalyst: the influence of carbon monoxide chemisorption on the topology of rhodium, J. Phys. Chem. 87 (1983) 2264–2267.
[50] X. Hong, B. Lim, Y. Wang, J. Lu, G. Hu, M. Luo, Stable Ir/SiO_2 catalyst for selective hydrogenation of crotonaldehyde, Appl. Surf. Sci. 270 (2103) (2018) 388–394.
[51] K. Bauer, D. Garbe, Common Fragrance and Flavor Materials, fifth ed., VCH, Weinheim, 1985, pp. 12–24.
[52] L. Massot, P. Palau, A. Savall, P. Taxil, Comparison between derived sol-gel and conventional methods for the preparation of dimensionally stable Ta/IrO_2 anodes for the oxygen evolution, J. New Mater. Electrochem. Syst. 10 (2007) 123–128.
[53] Haario Modest 6.0-A User's Guide. Prof. Math, Helsinki, (2001).
[54] D.P. Duarte, R. Martinez, L.J. Hoyos, Hydrodeoxygenation of 5-hydroxymethylfurfural over alumina-supported catalysts in aqueous medium, Ind. Eng. Chem. Res. 55 (2016) 54–63.
[55] T. Mallat, E. Orglmeister, A. Baiker, Asymmetric catalysis at chiral metal surfaces, Chem. Rev. 107 (2007) 4863–4890.
[56] D. Yu Murzin, P. Mäki-Arvela, E. Toukoniitty, T. Salmi, Asymmetric heterogeneous catalysis: science and engineering, Catal. Rev. Sci. Eng. 47 (2005) 175–256.
[57] X. Zuo, H. Liu, D. Guo, X. Yang, Enantioselective hydrogenation of pyruvates over polymer-stabilized and supported platinum nanoclusters, Tetrahedron 55 (1999) 7787–7804.
[58] Y. Nakagawa, M. Tamura, K. Tomishige, Supported metal catalysts for total hydrogenation of furfural and 5-hydroxymethylfurfural, J. Jpn. Petrol. Inst. 60 (1) (2017) 1–9.
[59] S. Nishimura, N. Ikeda, K. Ebitani, Selective hydrogenation of biomass-derived 5-hydroxymethylfurfural (HMF) to 2,5.dimethylfuran (DMF) under atmospheric hydrogen pressure over carbon supported PdAu bimetallic catalyst, Catal. Today 232 (2014) 89–98.
[60] P. Gallezot, D. Richard, Selective hydrogenation of α, β-unsaturated aldehydes, Catal. Rev. Sci. Eng. 40 (1&2) (1998) 81–126.
[61] T.T. Phuong, J. Massardier, P. Gallezot, Competitive hydrogenation of benzene and toluene on group VIII metals: correlation with the electronic structure, J. Catal. 102 (1986) 456–459.
[62] M.A. Barteau, Linear free energy relationships for C1-oxygenate decomposition on transition metal surfaces, Catal. Lett. 8 (1991) 175–183.
[63] C. Antonetti, D. Licursi, S. Fulignati, G. Valentini, A.M.R. Galletti, New frontiers in the catalytic synthesis of levulinic acid: from sugars to raw and waste biomass as starting feedstock, Catalysts 6 (12) (2016) 196.